A Study of Fog Clearing Using a CO_2 Laser

G. J. Mullaney,* W. H. Christiansen,† and D. A. Russell‡
Boeing Scientific Research Laboratories, Seattle, Wash.

It has been suggested that haze and fog may be dissipated by using a 10.6μ laser beam. This radiation is strongly absorbed by liquid water but only weakly absorbed by water vapor. Thus, the laser selectively deposits its energy in the water droplet, ultimately evaporating it. In this paper, the physics of fog removal by a CO_2 laser is explored, and the possibility of clearing airport runways is evaluated. Although initial estimates of the power required to clear a runway 10^6 to 10^7 w are large for present-day laser devices, they may not be excessive requirements for future systems.

I. Introduction

THE economic loss to the airlines in the United States due to the presence of fog at airports now amounts to 70 million dollars per year.[1] In a decade, this loss is predicted to increase to over 180 million dollars per year.[2] A number of methods for combating the problem have been tried, including fires, ultrasonic sound, and seeding.[3] It was recently pointed out that haze and fog may be cleared by using a CO_2 laser beam,[4] thus providing a new approach. 10.6μ radiation is strongly absorbed by liquid water because of an intermolecular bond which is not present in water vapor.[5] Indeed the difference between liquid water and water vapor on a per unit mass basis is approximately four orders of magnitude. Thus, the laser selectively deposits its energy in the water droplet, ultimately evaporating it. Such a scheme offers the prospect of a more efficient energy utilization than approaches that rely on heating large volumes of air.

In this paper, the physics of fog removal by a CO_2 laser is investigated and the possibility of clearing airport runways is evaluated. Laboratory measurements have been made of the evaporation rate of fog when subjected to an intensity of 5–300 w/cm^2 of 10.6μ radiation. An induced fog motion was detected during these experiments which led to a re-evaluation of the energy deposition process. Analysis shows that in the range of the experiments, a near-equilibrium evaporation of water takes place into the surrounding air. The clearing effectiveness of the laser under these conditions was also investigated with different fog densities, beam dimensions, and geometries.

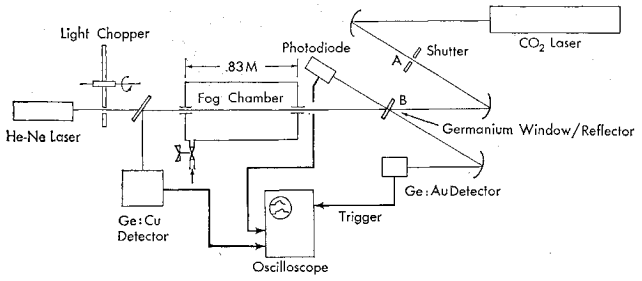

Fig. 1 Experiment arrangement for fog dissipation measurements.

Presented as Paper 69-670 at the AIAA Fluid and Plasma Dynamics Conference, San Francisco, Calif., June 16–18, 1969; submitted January 12, 1970; revision received April 20, 1970.

* Staff Scientist.
† Consultant, Aerospace Research Laboratory, University of Washington. Member AIAA.
‡ Consultant, Aerospace Research Laboratory, University of Washington. Member AIAA.

The results were extrapolated to airport dimensions and applied to the problem of clearing an airport runway of fog. Estimates of the power required to clear a specific volume to FAA specifications under various conditions of visibility and wind conditions were obtained. The calculations were compared with conditions at Seattle-Tacoma International and Los Angeles International airports using recorded meteorological data. Although the estimates of the power required to clear a runway are large for present-day laser devices, they may not be excessive requirements for future systems. A suggested geometry for a laser installation on a runway is described, and the economic feasibility is assessed.

II. Details of the Clearing Process

Experiments

The process of fog dissipation by CO_2 radiation was explored with a series of laboratory experiments. Reference 6 presented the initial results, including a study of the time to evaporate single fog droplets. The present study continues this work with emphasis on the scaling laws for fog clearing.

The experimental arrangement is shown schematically in Fig. 1. A small freezer was cooled to 275°K and steam introduced. Experiments were begun after the steam entry valve had been closed and the freezer had filled with a quiescent fog. A spherical mirror focused the output of the 10.6μ CO_2 laser (0–100w Coherent Radiation Laboratories Model 40) at point A, where a mechanical shutter provided an off/on switching time of 100μ sec. A second spherical mirror rendered the beam parallel with a 1.5-cm diam. Larger or smaller beams could be provided by insertion of a colimator after the second mirror. A germanium window (94% transmission) at B reflected a small portion of the CO_2 radiation to a Ge:Au detector, which could be used to start the oscilloscope sweep. The main beam passed through the fog chamber to a Ge:Cu detector.

Measurements of the clearing effectiveness of the CO_2 radiation were made by using a 0.63μ He–Ne laser as a visibility probe. This beam had a diameter of approximately 0.2 cm. It was chopped at 500 Hz and passed through the

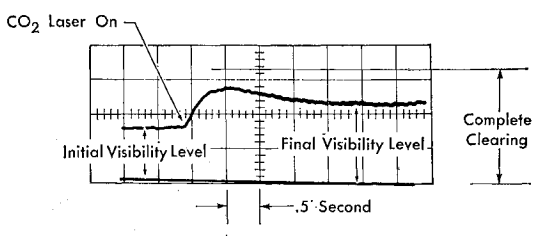

Fig. 2 Output of visibility probe (He-Ne beam).

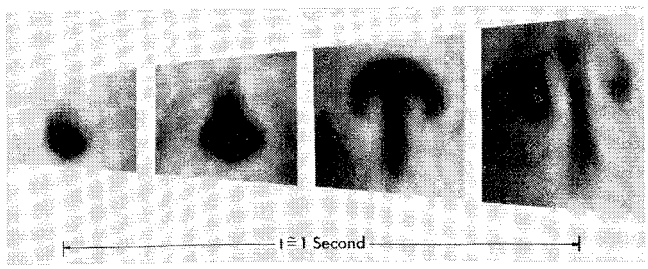

Fig. 3 Photographs of the clearing process taken at ¼-sec intervals.

fog chamber, generally along the axis of the CO_2 radiation. Most of the beam reflected off the germanium window and was then picked up by a photodiode, and the output was displayed on the oscilloscope. A typical oscillogram of the transmitted He–Ne signal is presented in Fig. 2. The lower line on this figure corresponds to zero transmitted signal, whereas the light upper line is the transmission without fog. The middle trace is the time dependent transmission of the He–Ne beam. It shows an increased transmission, corresponding to increased visibility, immediately after the CO_2 laser is turned on. The initial rise provides a measure of the droplet evaporation rate.[6] After a few seconds, the He–Ne signal becomes steady at a level which indicates improved visibility.

Figure 3 is a photograph taken along the beam axis using an intense white light beam to illuminate the fog. It shows the initial clearing of a hole in the fog by the CO_2 laser and the rise of a plume of cleared air as time progresses. Eventually the steady-flow condition is attained, for which 1–10 cm/sec plume velocities and 0.1–1°C plume temperature increases above ambient were measured. The convective motion reduces the length of time that a fog droplet is in the CO_2 beam, and thus limits the ability of the laser to completely clear the fog. In order to study this effect, measurements were made of the initial and final characteristic visibility lengths L_i and L_f as the CO_2 beam diameter d and power density P were varied.

L_i and L_f were obtained from the oscilloscope traces using the relation

$$I/I_o = \exp[-l/L] = \exp[-n2\pi r^2 l] \quad (1)$$

Here I/I_o is the attenuation of the He–Ne beam in passing through the fog chamber of length $l = 0.83$m. The attenuation is assumed to be caused by large particle scattering. The characteristic length is thus equal to $(n2\pi r^2)^{-1}$, where the particle density n, and the mean particle radius r, were estimated to be 10^3–10^4/cm^3 and 2–7μ, respectively.[6] L_i was set between 0.5m and 20m by varying the amount of steam admitted to the fog chamber prior to a test. P was varied between 5 and 300w/cm^2, whereas d was set at either 0.60, 1.50, or 2.85 cm. The data were taken with the He–Ne beam concentric with the CO_2 beam, with the common axis located a minimum of 15 cm from the sides and the top and bottom of the test chamber.

The data are presented in Fig. 4, where the ratio of initial to final visibility length is plotted vs the parameter $d^2P^2L_i$ (in w^2 per cm) for each experiment. The figure shows that L_i/L_f was always less than one and thus, that some fog clearing was realized under all experimental conditions. For fixed values of P and d, it can be seen that the light fogs (large L_i) showed the most improvement. With L_i fixed, increasing P or d also increased the clearing effectiveness. L_i/L_f and $d^2P^2L_i$ are seen to correlate the data.

Experiments designed to check the effect of a ground plane below the CO_2 beam did not produce significantly different results, unless the probing beam was moved close to the plane surface. More confined geometry would be expected to inhibit the induced motion and thus, improve clearing effectiveness. However, exploratory measurements produced inconclusive results, presumably as a result of thermal gradients introduced by the confining structures and the viscous nature of the flow.

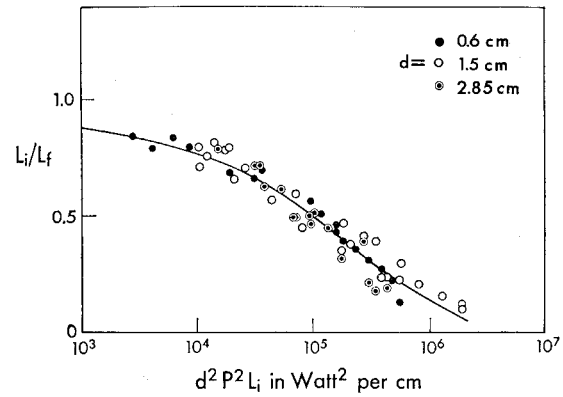

Fig. 4 Collected data from the fog clearing experiments [the solid curve is Eq. (6)].

Analysis

The rate of evaporation of a stationary fog is determined by a heat balance for the individual droplets. Some of the absorbed energy goes into evaporating the droplet and reducing its size, while the rest is conducted from the droplet surface to the surrounding air. It can be shown that[7]

$$r = r_i \exp[-t/\tau] \quad (2)$$

where r_i is the initial radius at $t = 0$. τ is a characteristic time for evaporation given by

$$\tau P = \text{const} = (3\rho h_v/\alpha)[1 + \mathfrak{L}] \quad (3)$$

where ρ is the liquid water density and h_v the heat of vaporization. α is the absorption coefficient for liquid water at 10.6μ, measured during the course of this study to be $0.12\mu^{-1}$. The second term in the brackets $\mathfrak{L}$ represents the loss due to heat conduction to the air. It was calculated to have a value of approximately 2 for the experimental conditions, independent of P (see Eq. 4, Ref. 6). Thus, $\frac{2}{3}$ of the absorbed laser energy goes into heating the air. This rise in air temperature is just that required by the Clausius-Clapeyron relation to prevent recondensation of the water vapor evaporated from the droplet.

If a mean value U is assigned as the induced steady flow through the CO_2 beam, Eqs. (1) and (2) give for L_i/L_f on the CO_2 beam centerline

$$L_i/L_f = (r_{d/2}/r_i)^2 = \exp\{-[2(d/2)/U\tau]\} = r_d/r_i \quad (4)$$

Here $r_{d/2}$ and r_d are the mean droplet radii after traversing distances $d/2$ and d from the beam edge. The convective flow pattern is complex: however, a useful result may be obtained if it is assumed that the kinetic energy in a "characteristic" volume in the flowing system is proportional to the energy that goes into heating the air in the same volume. This in turn is proportional to the amount of water vaporized from the droplets in the volume. Thus,

$$(\rho_{air} l d^2 U^2) \propto \mathfrak{L} h_v l d^2 n \rho (r_i^3 - r_d^3) = (\mathfrak{L} h_v l d^2/2\pi)(r_i/L_i)[1 - (L_i/L_f)^3] \quad (5)$$

ρ_{air} is used in calculating the kinetic energy, since the contribution from the water droplets is negligible. The last equality of Eq. (5) was obtained with the use of Eqs. (1) and (4). Inserting Eq. (5) into Eq. (4) and using Eq. (3),

$$(C/r_i)P^2 d^2 L_i = (l\eta L_i/L_f)^2[1 - (L_i/L_f)^3] \quad (6)$$

Equation (6) was fitted to the data of Fig. 4 by selecting

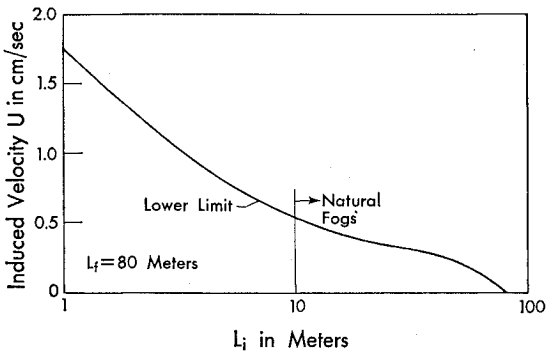

Fig. 5 Velocity induced by the clearing process vs the initial characteristic length L_i.

$C/r_i = 4.3 \times 10^{-6}$ cm/w^2. It is shown as the solid line on Fig. 4. The agreement is seen to be good for the complete range of the experiments, with no systematic differences observed. This suggests that r_i did not change markedly with L_i, although the logarithmic abscissa would obscure small variations. Equation (6) provides a simple exponential relation for small values of L_i/L_f, with a more complicated behavior as L_i/L_f approaches unity.

The experimental data are well correlated by Eq. (6), however, caution must be exercised when attempting to scale the results to much larger systems. The fraction of the kinetic energy to the total that is introduced by the laser is extremely small (of order 10^{-8}), and thus might be sensitive to small changes in the system or its scale.

III. Application to Airports

Having identified the physics of fog dissipation by a CO_2 laser, it is interesting to consider the possibility of clearing fog on a scale corresponding to an airport runway. Here the cleared volume must be large enough to visually land an aircraft (see Sec. IV), but as small as possible to minimize the laser power requirements. The dimensions used in the following analysis are 30m × 30m × 500m, where the longest dimension is taken as the runway length (l). The estimate of the power requirements to clear the volume is the subject of this section.

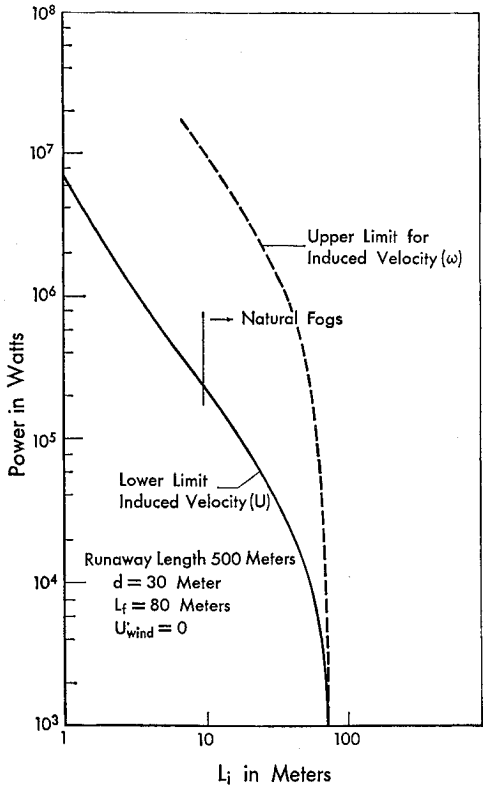

Fig. 6 Power required to clear the runway at zero wind speed.

The laser power requirements depend on the fog velocity, induced by the clearing process as well as by natural winds. Consider the laser power requirements due to the induced velocity. Using the results of Sec. II and combining Eqs. (3, 4 and 6) gives

$$U = [1 - (L_i/L_f)^3/(\tau P)^2(C/r_i)L_i]^{1/2} \quad (7)$$

The experimental value[6] of τP is 28 joules/cm^2. Equation (7) shows that U is independent of P and d, depending only on the degree of clearing L_i/L_f and the initial fog condition L_i.

The minimum requirement for Cat II-B landings is 1200-ft visibility (see Table 1, Sec. IV). Transmissometer calibration data[8] show that this corresponds to a value of L equal to 80 m). Using L_f = 80m, U can be calculated as a function of L_i. The resulting curve is shown in Fig. 5. U decreases with increasing L_i, going to zero at $L_i = L_f$ = 80m. It is small, being less than 1 cm/sec for natural fogs ($L_i >$ 10m). These low values of velocity may be questionable in view of the scale of the airport. It is possible that the induced flow changes character when scaled up to larger dimensions because of a Reynolds number effect. In our experiments the Reynolds number range was small ($3 < Re_d < 50$). Although Re dependence correlations were attempted, they were inconclusive. The authors believe the induced velocity U scaled from the experiments represents a lower limit on the induced velocity, with an upper limit not really known at this time. Using results of Scorer[9] for thermals, which are large Re flows, an upper limit can be estimated. From Scorer,

$$\omega = [(\tfrac{8}{9})g\bar{B}x]^{1/2} \quad (8)$$

where ω is the velocity of the thermal (interpreted to be the upper limit of induced velocity), g is the acceleration due to gravity, $\bar{B}$ is the mean buoyancy $\Delta\rho/\rho$, and x is the appropriate scale dimension normally taken as the half width of thermal. The effect of the nonuniform buoyancy and ground plane influence is here approximated by taking $\bar{B} = B_{max}/2$ (B_{max} is the buoyancy at 30m height) and using x as one-half the suggested dimension, i.e., $d/4$. B_{max} is given by $|\Delta\rho/\rho| = |\Delta T/T|$, since the pressure is constant. $\Delta T/T$ can be calculated knowing the heat loss during evaporation ($\mathcal{L}$ term effect) and setting this equal to the temperature rise in the surrounding air. It can be shown with this calculation that the ratio ω/U is a constant having a value of about 50 for a runway dimension of 30m. The upper limit induced velocity is less than 25 cm/sec for a typical fog.

The laser power required to clear the runway $\bar{\mathcal{P}}$ was calculated by equating it to the rate of energy required to evaporate the fog drops as they are carried through the runway volume by the induced wind;

$$\bar{\mathcal{P}} = Pd^2 = dl\rho h_v[1 + \mathcal{L}]n\tfrac{4}{3}\pi[r_i^3 - r_d^3]U \quad (9)$$

Table 1 Low-visibility landing categories

Category	Runway visual range (RVR)	Decision height (DH)[a]
	ft	ft
I	2400	200
II-A	1600	150
II-B	1200	100[b]
III-A	700	...
III-B	150	...
III-C	0	...

[a] A height (above runway elevation) below which a pilot must not descend if he has not obtained adequate visual references *before* approaching this point. He must execute a missed-approach procedure at this point or be assured he has adequate references to land by visual means.
[b] Sometimes called CAT II.

This equation assumes a geometry can be realized whereby all the laser radiation is absorbed within the volume. Equation (9) can be rewritten with the help of the previous equations as

$$\mathcal{P} = \tfrac{2}{9}\alpha d l(r_i/L_i)[1 - (L_i/L_f)^3]^{3/2}/[(C/r_i)L_i]^{1/2} \quad (10)$$

Considering $r_i = 5\mu$ as an average value of the drop radius and d the width of the runway, the required power can be calculated. Figure 6 shows $\mathcal{P}$ as a function of L_i for $L_f = 80$. The power is a maximum for low values of visibility and is zero at $L_i = 80$m. If the upper velocity ω is used, the power requirements are higher as shown by the dashed line in Fig. 6.

Wind loads must also be considered as they are often larger than the induced velocity. For winds perpendicular to the runway, a heat balance identical to Eq. (9) can be used if U is replaced by $U_{w\perp}$;

$$\mathcal{P}_{w\perp} = \mathcal{P}(U_{w\perp}/U) \quad (11)$$

where the subscript $w_\perp$ represents wind perpendicular to the runway. For winds parallel to the runway, the cross-sectional area used in calculating the flux of fog across the runway changes so as to reduce the power required. Thus,

$$\mathcal{P}_{w_{||}} = \mathcal{P}(d/l)(U_{w\perp}/U) \quad (12)$$

where the subscript $w_{||}$ represents wind parallel to the runway. Power calculations for dense natural fogs ($\frac{2}{16}$-mile visibility range) are shown in Fig. 7, together with the zero wind calculations. The power requirements are linear with wind speed, the parallel wind requirement being the lower by a factor of $\frac{3}{50}$ as a result of area change. Even for low-wind speeds, say 100 cm/sec (approximately 2 knots) the power requirements are large, especially for the perpendicular wind case. Fortunately, airports are usually designed with the runways parallel to the local wind trends, thus reducing the possible times that winds blow across runways. For a general wind direction the total power requirement $\mathcal{P}_T$ may be approximated by

$$\tilde{\mathcal{P}}_T = \tilde{\mathcal{P}} + \tilde{\mathcal{P}}_{w\perp} + \tilde{\mathcal{P}}_{w_{||}} = \tilde{\mathcal{P}}\left[1 + \frac{U_w \sin\theta}{U} + \frac{d}{l}\frac{U_w}{u}\cos\theta\right] \quad (13)$$

where the wind has been resolved into perpendicular and parallel components and θ is measured from the runway direction. This equation can be used to estimate the power required to clear an airport. Equation (13) is a function of U_w, θ, and L_i for fixed L_f.

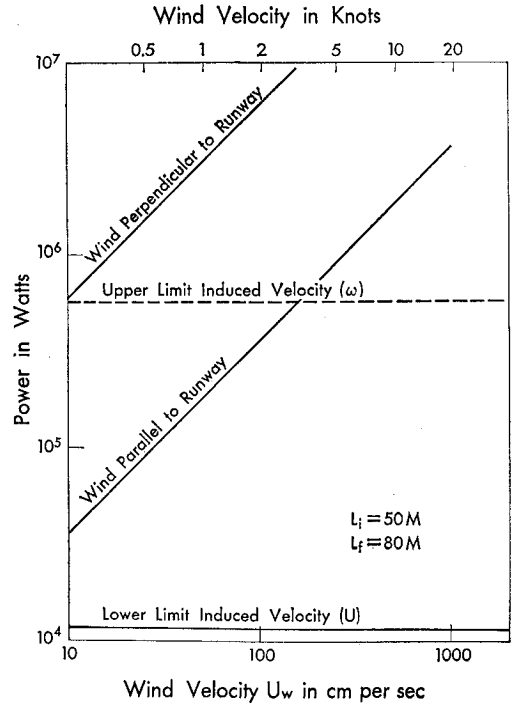

Fig. 7 Power required to clear the runway vs wind velocity.

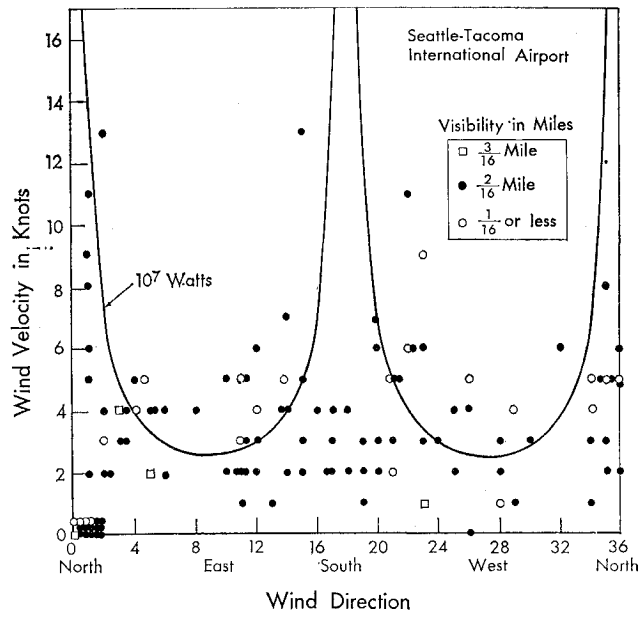

Fig. 8 Meteorological conditions at Seattle-Tacoma International Airport during fog.

Recorded meteorological data[10] for the years 1965–1968 were used to obtain wind speed and direction relative to the runway when there was a significant fog ($L_i < 80$m) for two selected airports (Los Angeles International and Seattle-Tacoma International). The visibility, measured in $\frac{1}{16}$ of a mile, was noted as well. This information was plotted on a graph of wind speed (knots) vs the wind direction in degrees. The degree of fog intensity (proportional to the inverse of visibility) is noted on the graph by different symbols. The data for Seattle-Tacoma International Airport is plotted in Fig. 8, while Los Angeles data is shown in Fig. 9.

Using a 10^7-w source at the airports, the wind speed and direction that can be handled by the laser beam for category

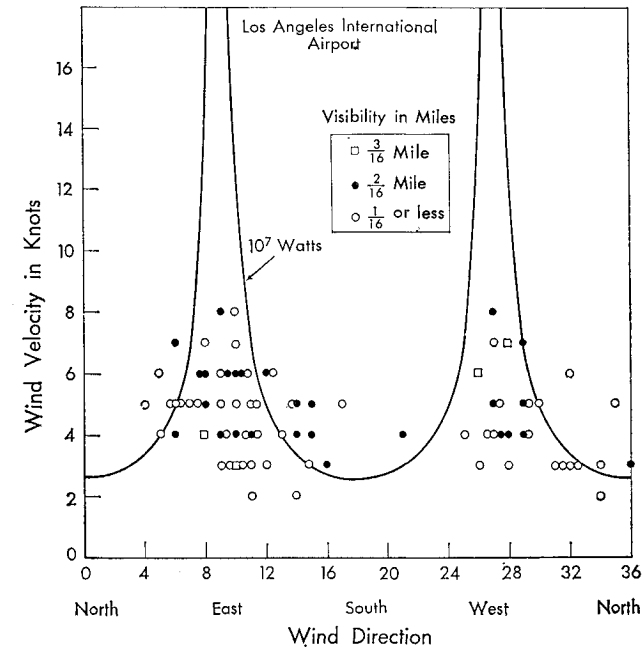

Fig. 9 Meteorological conditions at Los Angeles International Airport during fog.

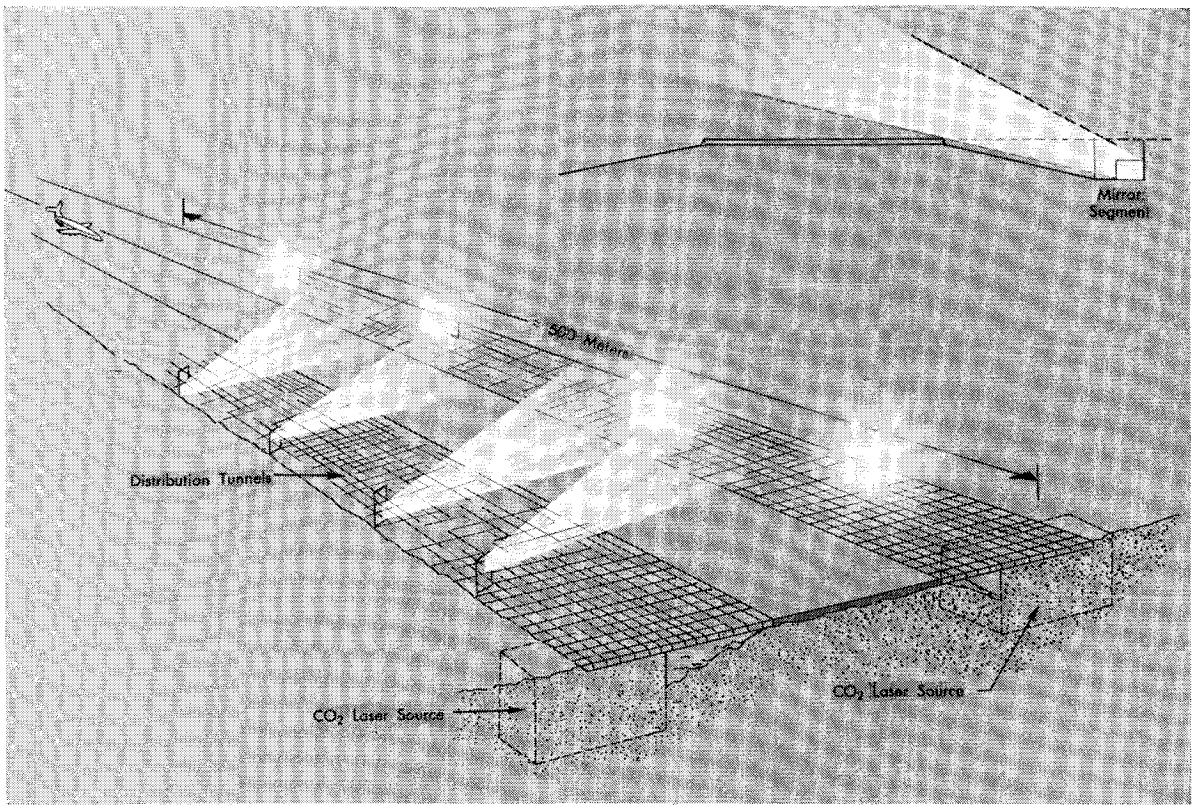

Fig. 10 Suggested laser system for fog clearing of an airport runway.

II-B landings can be calculated from Eq. (13) if L_i is known. Seattle-Tacoma fogs are seen to be predominately $\frac{2}{16}$ mile visibility or $L_i = 51$m, which was taken as the average fog. Using $L_i = 51$m the tolerable wind speed vs direction (measured from the runway) was calculated. The results are shown by the curve in Figs. 8 and 9. The peaks in these curves represent wind directions along the runway, whereas the minimums represent wind directions perpendicular to the runway. Data points falling below these curves represent fogs at these airports which are cleared by the laser beam. Conversely points above these curves cannot be completely cleared by the use of the laser. In both cases, a 10^7-w laser can clear 80% of the serious fogs that occur at these airports, whereas twice this power can clear essentially all fog. Fogs with little or no wind associated with them are handled very easily (cf Fig. 6). Radiation fogs such as those that exist at Dulles International Airport may represent this case. However, meteorological data recorded for this airport is still sparse and no calculations could be made.

IV. Airport Laser System

At this time the airlines and the major airports are upgrading to category II weather operation. The different categories of landing minimums are defined in Table 1.

With present equipment there is an unacceptably low approach success under category II-B weather,[11] and the lowest range of category III operation is years away. In the United States, the philosophy continues to be that the pilot actively controls landing of the aircraft. The procedure under adverse weather conditions during a landing is to initially rely on instrumentation, change over to visual observations, then return to a combination of both during the most critical stage of the landing. Better systems are needed to strengthen the visual portion of the landing operation.

As shown in Sec. III, a laser power of 10^7 w can clear most fogs (either warm or cold), to meet the visibility requirements for an FAA category II-B landing. Time to improve visibility would be about 60 sec. The laser system would be combined with category II ground and airborne equipment to permit aircraft movements under category II and III weather conditions.

A sketch of a suggested fog clearing system is shown in Fig. 10. Power plants installed underground on each side of the runway would energize the laser system. The output CO_2 laser beams would travel from the power plant in distribution tunnels parallel to and below the runway. Reflecting mirrors at several stations would also expand the beam and rapidly reduce its intensity as it passed through a grating adjacent to the runway. The radiation intensity level in the zone through which the aircraft would pass would be 10 times that of sunlight, 1 w/cm^2 and would not present a safety problem. During landing the flare begins when the aircraft wheels are 15 m above the ground. The ideal touchdown distance with a 3° glide path is 290 m with a touchdown dispersion of perhaps ±150 m. Thus, a 500-m path length along the runway cleared by the laser would provide a minimum acceptable visibility distance during the critical phase for landing.

The equipment costs for such an installation might be similar to gas turbine electrical generators of the same power output (100 dollars per 10^3 w). Thus, the laser power source would be a million dollar investment. All weather landing systems of the more conventional type for category III-A and III-B conditions have comparable costs. Any system would require an additional investment in ground equipment for surface routing of aircraft during III-B or III-C weather conditions.

A recent study done by a consultant firm[2] for the FAA projects much heavier air traffic loads to come in the next decade. Net economic benefits will be possible to the airlines and the national economy by upgrading the aircraft equipment and ground installations on the forty major airports. The benefit/cost ratios which would result from installing equipment for all weather landing systems are favorable. Combining a laser with present systems would provide the same favorable economics. Thus, laser systems may become an integral part of future all-weather landing systems.

References

[1] Halaby, N. E., "All Weather Operations—Progress and Challenges," *Astronautics and Aeronautics*, Vol. 6, No. 5, May 1968, pp. 63–69.

[2] Speas, R. D. et al., "Cost/Benefit Analysis for All-Weather Landing Systems," Rept. RD-67-28, Oct. 1967, System Research and Development Service of F. A. A., Manhasset, N.Y.

[3] Beckwith, W. B. and Harrison, H. T., "The History and Status of Artificial Fog Dispersal," Rept. 110, Jan. 1964, United Airlines, O'Hare International Airport, Chicago, Ill.

[4] Townes, C. H., private communication, Professor of Physics at Large, University of California, Berkeley, Calif., Jan. 1968.

[5] Kondrat yev et al., "The Infrared Absorption Spectrum of Water in its Liquid State," TTF-211, July 1964, NASA.

[6] Mullaney, G. J., Christiansen, W. H., and Russell, D. A., "Fog Dissipation Using a CO_2 Laser," *Applied Physics Letters*, Vol. 13, No. 4, Aug. 15, 1968, pp. 145–147.

[7] Williams, F. A., "On Vaporization of Mist by Radiation," *International Journal of Heat Mass Transfer*, Vol. 8, 1965, pp. 575–587.

[8] *Instruction Book for Transmissometers*, AN/TMQ-10 NBS Rept. 2588, revised 1959, National Bureau of Standards, Washington, D.C.

[9] Scorer, R. S., "Experiments on Convection of Isolated Masses of Buoyant Fluid," *Journal of Fluid Mechanics*, Vol. 2, 1957, pp. 583–594.

[10] "Local Climatological Data Charts, Data Obtained for Several Airports," 1965–1968, National Weather Records Center, Asheville, N.C.

[11] Litchford, G. B., "Low-Visibility Landing," *Astronautics and Aeronautics*, Vol. 6, No. 11, Nov. 1968, pp. 26–38.

FEBRUARY 1971 J. AIRCRAFT VOL. 8, NO. 2

Use of Ground Based Simulators in Aircraft Design

P. G. Dillenschneider* and A. W. Shaw†
LTV Aerospace Corporation, Dallas, Texas

The growth in flight simulation technology in the flight training context and the extension of this technology to engineering oriented flight simulation is discussed briefly. Basic differences between simulation used for training and engineering design are identified. The use of ground based flight simulation in support of aircraft design is demonstrated by presenting three diverse but typical examples. The specific engineering oriented simulations discussed are an air combat simulation used to evaluate the effect of changes in gross aircraft characteristics on air combat effectiveness, the approach and landing on board an aircraft carrier at night to evaluate aircraft handling qualities in this critical tracking task, and a V/STOL assault transport simulation used to tailor aircraft dynamics, control feel system characteristics and flying qualities over the complete aircraft flight envelope.

Introduction

SOPHISTICATED ground based flight simulation has been in general use since the advent of real time electronic analog computers. Over the past decade great strides have been made in improving the fidelity of flight simulators associated with training, through the rapid development of hybrid/digital computers and the associated environmental devices—principally cockpit motion and real world visual display systems. Application of this technology to the engineering design task has added a new dimension to the analysis and synthesis of flight systems.

The flight training simulator is used to promote a change in behavior through practice in the simulated flight environment. The simulator, normally restricted to the representation of a single aircraft over a well-defined flight regime, becomes available only after the design of the aircraft is completed.

The engineering simulator, on the other hand, is used in the very early stages of the design cycle to establish aircraft and aircraft systems design requirements and the evaluation of alternative approaches to the solution of engineering design problems. Typical engineering tasks include the assessment of flying qualities, evaluation of flight control feel systems, study of stabilization and automatic flight control systems, determination of the significance of gross aircraft design parameters, appraisal of crew station configurations, development of cockpit displays, exploration of head-up display symbology, evaluation of system failure modes and emergency conditions, etc. The simulator, normally configured on a very short time scale by the use of flexible hardware and software "building blocks," has a brief life span in any particular configuration. An individual program is nearly always devoted to the study of a single design problem. The fidelity of the mathematical model of the aircraft and its systems and the environmental devices employed are largely dictated by the status of the particular design. Early in the design, the mathematical models are generally first order approximations. As the design progresses, the fidelity of the mathematical models are improved appropriately—ultimately including all major nonlinearities which might affect design decisions. In a similar manner, the environmental devices employed extend over the full range of fidelity. Therefore, throughout the research and development phase of an aircraft or aircraft system one is likely to see a wide range of simulation fidelity—ranging from very simple single degree of airframe freedom, restricted maneuvering range, fixed base, instrument flight studies to full 6° of airframe freedom, maneuvering over the complete flight envelope, realistic cockpit mounted on a motion system, and employing a real world visual display.

Numerous examples of the use of ground based flight simulation in support of aircraft design are evident throughout the aircraft industry, Department of Defense laboratories, and the NASA. Several typical examples of engineering oriented flight simulation studies, recently conducted at the Vought Aeronautics Company, LTV Aerospace Corp., are presented below.

Submitted March 4, 1970; revision received June 13, 1970. Part of this work was accomplished under Contract Numbers N00019-68-C-0075 and AF33(657) 7868.

* Supervisor, Flight Simulation, Vought Aeronautics Division. Associate Fellow AIAA.

† Chief of Aerodynamics, Vought Aeronautics Division. Associate Fellow AIAA.